JOURNAL OF
PEPTIDE SCIENCE

Temperature and pH effects on biophysical and morphological properties of self-assembling peptide RADA16-I‡

ZHAOYANG YE,[a][§] HANGYU ZHANG,[a][§] HANLIN LUO,[a][§] SHUNKANG WANG,[a] QINGHAN ZHOU,[a] XINPENG DU,[a] CHENGKANG TANG,[a] LIYAN CHEN,[a] JINGPING LIU,[a] YING-KANG SHI,[b] ER-YONG ZHANG,[b] RUTLEDGE ELLIS-BEHNKE[c,d] and XIAOJUN ZHAO[a]*

[a] Institute for NanoBiomedical Technology and Membrane Biology, West China Hospital, Sichuan University, Science Park No 1, Ke Yuan 4th St., Gao Peng Road, Hi-tech Industrial Development Zone, Chengdu, 610041, Sichuan, China
[b] West China Medical School, West China Hospital, Sichuan University, Guo Xue Xiang 37, Chengdu, 610041, Sichuan, China
[c] Department of Brain & Cognitive Sciences 46-6007, Massachusetts Institute of Technology, 77 Massachusetts Avenue of Technology, MA 02139-4307, USA
[d] Department of Anatomy, Li Ka Shing Faculty of Medicine, University of Hong Kong, 1/F Laboratory Block, 21 Sassoon Road, Pokfulam, Hong Kong SAR, China

Abstract: It has been found that the self-assembling peptide RADA 16-I forms a β-sheet structure and self-assembles into nanofibers and scaffolds in favor of cell growth, hemostasis and tissue-injury repair. But its biophysical and morphological properties, especially for its β-sheet and self-assembling properties in heat- and pH-denatured conditions, remain largely unclear. In order to better understand and design nanobiomaterials, we studied the self-assembly behaviors of RADA16-I using CD and atomic force microscopy (AFM) measurements in various pH and heat-denatured conditions. Here, we report that the peptide, when exposed to pH 1.0 and 4.0, was still able to assume a typical β-sheet structure and self-assemble into long nanofiber, although its β-sheet content was dramatically decreased by 10% in a pH 1.0 solution. However, the peptide, when exposed to pH 13.0, drastically lost its β-sheet structure and assembled into different small-sized globular aggregates. Similarly, the peptide, when heat-denatured from 25 to 70 °C, was still able to assume a typical β-sheet structure with 46% content, but self-assembled into small-sized globular aggregates at much higher temperature. Titration experiments showed that the peptide RADA16-I exists in three types of ionic species: acidic (fully protonated peptide), zwitterionic (electrically neutral peptide carrying partial positive and negative charges) and basic (fully deprotonated peptide) species, called 'super ions'. The unordered structure and β-turn of these 'super ions' via hydrogen or ionic bonds, and heat Brownian motion under the above denatured conditions would directly affect the stability of the β-sheet and nanofibers. These results help us in the design of future nanobiomaterials, such as biosensors, based on β-sheets and environmental changes. These results also help understand the pathogenesis of the β-sheet-mediated neuronal diseases such as Alzheimer's disease and the mechanism of hemostasis. Copyright © 2008 European Peptide Society and John Wiley & Sons, Ltd.

INTRODUCTION

The design, synthesis and fabrication of biological nanomaterials, such as nanofibers and scaffolds based on a 'bottom-up' self-assembly peptide system, have attracted a great deal of attention from biomaterials and nanobiotechnology researchers for their potential applications in nanobiotechnology and biomedical engineering [1–21]. For example, the 16-residue peptide, RADARADARADARADA (RADA16-I), was designed and synthesized by mimicking the amphiphilic segment of EAEAKAKAEAEAKAKA (EAKA 16-II) of the naturally occurring yeast Zuotin protein. This ionic-complementary peptide contains a regular repeat of alternating hydrophobic and hydrophilic amino acids, including positively and negatively charged residues being arranged alternatively (Figure 1).

RADA 16-I is able to self-assemble into scaffolds, composed of interwoven nanofibers with ~100-nm mesh pores, in a way that mimics naturally occurring extracellular matrix (ECM), thus supporting cell and tissue growth, and consequently tissue-injury repair. For example, this peptide matrix has been shown to support rat hippocampal cell cultures, allowing for proliferation and differentiation, as well as synaptogenesis, in the RADA scaffold [5]. In addition, the nanomaterial has also been reported to repair the optic tract in Chinese hamsters and act as an effective hemostatic medicine [22].

* Correspondence to: Xiaojun Zhao, Institute for NanoBiomedical Technology and Membrane Biology, West China Hospital, Sichuan University, Science Park No 1, Ke Yuan 4th St., Gao Peng Road, Hi-tech Industrial Development Zone, Chengdu, 610041, Sichuan, China; e-mail: Zhaoxj@scu.edu.cn; xiaojunz@mit.edu
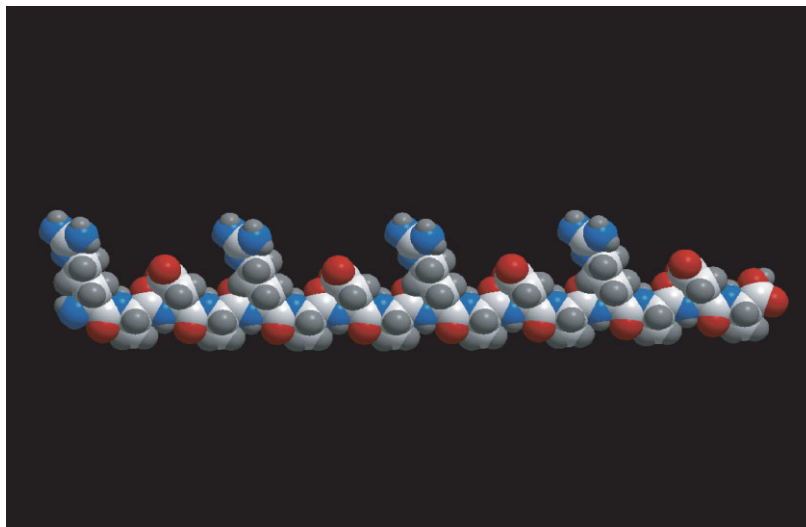
Figure 1 Schematic representation of three-dimensional molecular model of peptide RADA16-I. Carbon atoms are white, oxygen atoms are red, nitrogen atoms are blue, and hydrogen atoms are gray. In this conformation, all the hydrophobic alanine side chains face in one direction, and all the arginine and aspartic acid side chains face in the other direction to produce two different faces. On the polar side, arginine acid alternates with aspartic acid. The dimensions are about 5 nm in length, 1.3 nm in height, and 0.8 nm in width [28].

Self-assembly is a spontaneous process by which many individual molecules are associated into a coherent and organized structure under thermodynamic equilibrium conditions by noncovalent interaction, such as ionic and hydrogen bonding [23–38]. The peptide RADA 16-I forms a stable β-sheet structure in water and further self-assembles spontaneously into three-dimensional scaffolds in the presence of monovalent cations or physiological conditions [23]. Although this peptide has been widely used for cell- and tissue-related work, its biophysical properties and self-assembly mechanism have not yet been fully characterized. In this study, we examined the biophysical and morphological properties of its β-sheet structure and its self-assembled nanofibers under pH- and heat-denatured conditions using CD and atomic force microscopy (AFM) techniques. Our data demonstrated that peptide RADA 16-I self-assembled into very strong β-sheet structures, which were either fully or partially maintained under most extreme pH- and heat-denatured conditions. The β-sheet structure, after being extremely heat-denatured, was able to reassemble into the β-sheet structure. Peptide RADA 16-I behaved like a 'super ion' interacting with itself via intra- and intersalt bridges to stabilize the β-sheet and the self-assembled nanofiber structure.

MATERIALS AND METHODS

Peptide

Peptide RADA16-I (PuraMatrix™, $CH_3CO-NH-(Arg-Ala-Asp-Ala)_4-CONH_2$, 1% w/v, theoretical mass = 1712.9) was purchased from 3DM Inc (Cambridge, MA), stored at 4 °C, and used without further purification. Peptide stock solutions were made of 0.1% (w/v) with Milli-Q water (18.2 MΩ) and stored at 4 °C before use. For measurement of active isoelectric point (pI), 0.1 M HCl and/or 0.1 M NaOH were used and mixed with the peptide stock solution to give a final peptide concentration of 0.17 mg/ml (100 μM). An aliquot of 600 μl was tested using the Mettler Toledo pH meter SG2 for pH measurement. The samples were incubated at room temperature overnight prior to AFM imaging and CD measurement.

Heparin-Treated Blood of Rabbit

An aliquot of 2 ml fresh blood harvested from adult New Zealand white rabbits ear artery with about 3 kg in weight (located at the Center of Laboratory Animals of Clinical Medicine School of Sichuan University) was subsequently mixed with an aliquot of 2 μl heparin (3000 U/ml). The heparin-treated (18 U/ml) blood of rabbit was stored at 4 °C before use. For AFM, half of the heparin-treated (18 U/ml) blood of rabbit was mixed with half of the peptide RADA16-I (10 mg/ml).

Measurement of Apparent pK1, pK2, and Active Isoelectric Point (pI) of Peptide RADA16-I

The pH of the peptide solutions was measured by a glass microelectrode, which is attached in the Mettler Toledo pH meter SG2. Before use, the pH meter was calibrated by a 3-point calibration with attached pH 4.01, 9.21, and 10.01 calibration buffers according to commercial protocols. Aliquots of 600 μl (100 μM) peptide RADA16-I aqueous solution were applied for measurement and an appropriate amount of acid (0.1 M HCl) or base (0.1 M NaOH) was added each time with a pipette, followed by microvortex oscillator for about 5 s. The pH determination was performed with pH meter at least five times with ±0.1 pH variation at room temperature (25 °C) and the curve of pH as the function of cumulative molarity of acid

or base was determined. The apparent pK_1, pK_2, and active pI of peptide RADA16-I were all determined, according to the related formulae described in textbook.

CD Measurement

All CD spectroscopy was performed on the peptide (100 μM) solutions (pure water and 0.1 M HCl or 0.1 M NaOH) that were incubated at 4 °C overnight. CD data were gathered on an Aviv model 400 spectrophotometer with 0.001–0.2 millidegrees sensitivity and a 2-mm pathlength quartz cuvette (Hellma Standard Cuvet 110QS (Quartz Suprasil)). The supported parameters: $\lambda = 260$–190 nm, $\triangle \lambda$ (bandwidth) = 1 nm, time constant = 1 s, using 3-times scans for average. Be sure to check the baseline CD signals of the empty cuvette and record a baseline spectrum of the cuvette containing only pure water under identical conditions.

CD data were corrected by conversion to mean-residue ellipticity to account for slight differences in molecular weight and concentration. The effects of pH and temperature on peptide structure were determined by taking CD scans at different pH (1.0, 4.0, 7.0, and 9.5) and different temperatures ranging from 25 to 80 °C.

The position and the relative magnitude of the minimum-mean-residue ellipticity were monitored to evaluate the β-sheet structures and their relative β-sheet content of peptide RADA16-I at various environments.

In order to fully investigate the effect of pH and temperature on secondary structures and self-assembling nanofiber formation of peptide RADA16-I, a free software CDPro (http://lamar.colostate.edu/~sreeram/CDPro/main.html) was applied to estimate secondary-structure contents. The peptide secondary-structure fractions at various environments were calculated by the modified Contin method (CONTINLL program) with comparison to selected reference proteins set (IBasis7 (SDP48), $\lambda = 240$–190 nm). The calculated CD spectral data were compared with the experimental CD spectrum with little difference (data not shown), and the amount of the root-mean-square deviation (RMSD) and the normalized-mean-square deviation (NMRSD) between the both are close to 0.1 and zero (Tables 2 and 3), respectively, suggesting that CONTINLL program and SDP48 fitting are suitable for CD analyses of peptide RADA16-I.

Atomic Force Microscopy (AFM)

An aliquot of approximately 5 μl of the peptide (0.17 mg/ml) solution, heparin-treated (18 U/ml) blood, or heparin-treated (18 U/ml) blood mixture (1 : 1 v/v) with peptide RADA16-I (10 mg/ml), was evenly placed on the surface (about 10 mm × 10 mm square or 15-mm diameter) of a freshly cleaved mica surface. Each sample was left on the mica for about 30 s and then rinsed with aliquots of 100 μl of Milli-Q water to remove unattached peptides or blood cells. The sample on the mica surface was then air-dried for AFM observation.

AFM was performed with a SPI4000 Probe Station & SPA-400 SPM Unit (Seiko Instruments Inc., Chiba, Japan) using the dynamic force mode. The images utilized a 20-μm scanner (400) and an Olympus Si-DF20 microcantilever as well as a Si tip of radius 10 nm, rectangular base 200.00 μm, with tip height of 10.00 μm and spring constant Kz of 12.00 N/m. The cantilever's free resonance frequency (Fo) was 127.00 kHz,

and the applied frequency (the working point) was set on the lower side of the resonance frequency (the left side of the Q Curve), accompanied by the cyclic contact mode. All of the measurements were performed in ambient air. Height images were recorded with 512×512 pixels resolution, in which the brightness of morphology increases as a function of height and the main parameters of AFM observation were as follows: Amp. Ref. (amplitude reference): -0.15 to -0.35, I Gain/P Gain (integral gain/proportional gain): 0.10–0.33/0.05–0.15, Amplitude: ~1 V, scan speed: 0.5–1.5 Hz. All image data sets were subjected to first-order flattening, in order to correct for the tilt of the selected area and cancel any distortion (reversal) of causeless drifting or vibration (creeping) of the scanner. The AFM observation of each sample was repeated at least four times.

To quantitatively analyze the data, a large amount of the images has been examined in order to find the surface coverage of nanofibers, clusters and branches and further calculate the length of nanofibers. In higher magnification images, the width and height of nanofibers can be determined using SPI3800N-offline image analysis program for win2000 software, also called as 'SPIWin'.

Phase-imaging AFM can simultaneously monitor the change of the phase lag of the oscillation frequency of microcantilever with different visualized pixels, when performing height-imaging AFM at the tapping mode. One of distinguished characterizations for phase imaging is its high sensitivity for the change of morphology [39]. Therefore, phase-imaging AFM has been employed to discriminate overlapping between blood cells and peptide RADA16-I in order to detect the morphological change of blood cells surface. The red and white blood cells are identified by their conventional scanning electron microscopy (SEM) images described in textbook.

RESULTS

Measurement of the Apparent pK1, pK2, and the Isoelectric Point (pI) of Peptide RADA16-I

The molecular model of peptide RADA16-I is shown in Figure 1. This peptide contains four acidic residues of aspartic acid ($pI = 2.77$, $pK_R = 3.65$), four alkaline residues of arginine ($pI = 10.76$, $pK_R = 12.48$), and eight alanine ($pI = 6.00$) residues. The titration experiment showed that this peptide has a similar titration curve, when compared to that of a general nonpolar amino acid. An abrupt change in its apparent pI of about 7.20 was detected (Figure 2). Further analysis indicated that the apparent pK of four acidic aspartic acid residues was defined as $pK_1 \approx 1.79$, which is much lower than pK_R (3.65) of aspartic acid with about 100 times active acidic ion concentration increase. The apparent pK_2 of four alkaline arginine residues was about 12.58 with little alkaline enhancement mainly because of high stability of the strong basic guanidinium substituent. The different ions states (Table 1, and Figure 3) of peptide RADA16-I are distinguished by the apparent $pK1$, $pK2$, and pI.
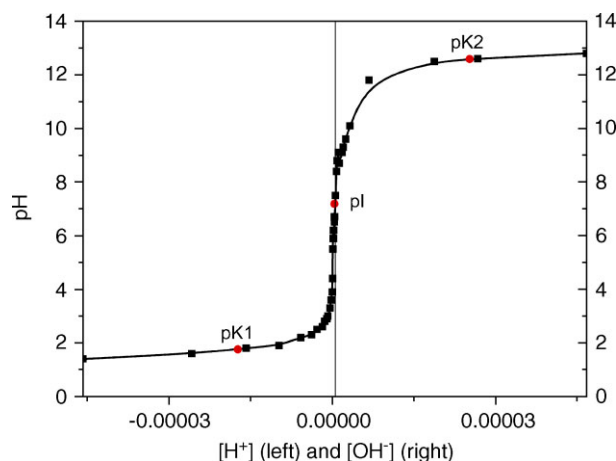
Figure 2 Active isoelectric point (pI) of peptide RADA16-I. The curve of the pH as the function of corresponding cumulative molarity of acid or base was determined. The apparent p$K_1 = 1.79$ of side chains carboxyl (–COOH) of aspartic acid residues was extracted at the inflexion of the basic titration curve(left) and the apparent p$K_2 = 12.58$ of arginine residues side chains at the inflexion of the acidic titration curve(right). The active p$I = 7.20$ of peptide RADA16-I can be calculated from the formulation of p$I = (pK_1 + pK_2)/2$. This figure is available in colour online at www.interscience.wiley.com/journal/jpepsci.

Effect of pH on Nanofiber Formation

The pI of peptide RADA 16-I was about 7.20 and the β-sheet structure would be impaired in the extreme pHs. Surprisingly, CD measurements (Figure 4) showed that peptide RADA16-I (100 μM) was able to adopt its typical β-sheet structure (minimum at 217–218 nm and maximum at 195–206 nm) in pH = 1.0–9.5 solutions, which could also be evidenced by 44.7–54.3% high β-sheet contents (Table 2, S(r) + S(d)), according to CDPro software analyses. However, when the pH was changed from 4.0 to 9.5, there were about 10.5% decrease of the β-sheet contents with about 15.1% increase of the unordered structure content to almost zero contents

(Table 2, H(r) + H(d)) maintaining of α-helix. These data indicated that the β-sheet structure was impaired to a different extent at different pH values and its β-sheet content was more compromised at the extreme pH values, respectively.

AFM morphological studies demonstrated that the nanofibers in pH 1.0 (Figure 5(A–C)) and 4.0 (Figure 5(D–F)) solutions were about 17.5 ± 1.13 nm in width, 1.4 ± 0.36 nm in height, and 1108 ± 184 nm in length, which are consistent with previous reports [1–6]. Moreover, smaller sized ~100–500 nm nanofibers (Figure 6(A)) or aggregates (Figure 6(B–E)) have been detected in pH 4.5–9.5 solutions. Furthermore, even smaller globular aggregates of ~50 nm widths (Figure 6(F)) have also been observed in pH 13.0 condition. Usually, a good β-sheet structure helps peptides to self-assemble into nanofiber, but surprisingly, peptide RADA16-I in pH 9.5 and 13.0 with certain β-sheet structure did not form good nanofiber (Table 2, Figure 6), strongly indicating that the β-sheet structure is essential but not sufficient for fiber self-assembly. These data also indicated that higher β-sheet contents and lower unordered structure are required for nanofiber formation.

Table 1 Ion states in peptide RADA16-I solution at 25 °C

pH(pK)	[(II)]/[(I)]	[(II)]/[(III)]	Major ions
1.0	1/6		$H^+, I^+ > II^{+,-}$
1.8	1/1		$H^+, I^+ \approx II^{+,-}$
4.0	160/1		$H^+, I^+ < II^{+,-}$
7.2		Isoelectric point	$OH^-, II^{+,-}$
9.6	1260/1		$OH^-, II^{+,-} >> III^-$
12.6		1/1	$OH^-, II^{+,-} \approx III^-$
13.0		2/5	$OH^-, II^{+,-} < III^-$

Table 2 Estimated structure fractions of peptide RADA16-I in various pH values

Items	RMSD/NRMSD	Secondary-structure fractions (%)[a]					
		H(r)	H(d)	S(r)	S(d)	Turn	Unrd
pH = 4.0	0.113/0.054	1.3	3.0	39.2	15.1	20.7	20.7
pH = 1.0	0.041/0.039	0.3	3.2	30.2	14.5	21.6	30.2
pH = 7.0	0.111/0.160	0.2	1.8	31.5	13.6	17.0	35.8
pH = 9.5	0.087/0.124	0.3	2.1	31.1	14.5	18.7	33.3
Deviation(+/−)[b]		0.0/1.1	0.2/1.2	0.0/9.0	0.0/1.5	0.9/3.7	15.1/0.0

[a] Including six types of secondary structures: H(r) is regular α-helix; H(d) is distorted α-helix; S(r) is regular β-strand; S(d) is distorted β-strand (a partial, but far from complete distortion of the regular β-strand because of the lack of some hydrogen bonds); Turn is β-turn structure; Unrd is unordered structure.
[b] The maximum increase (+) and decrease (−) of secondary-structure fractions (%) compared with those at pH = 4.0 (pure water, 25 °C).
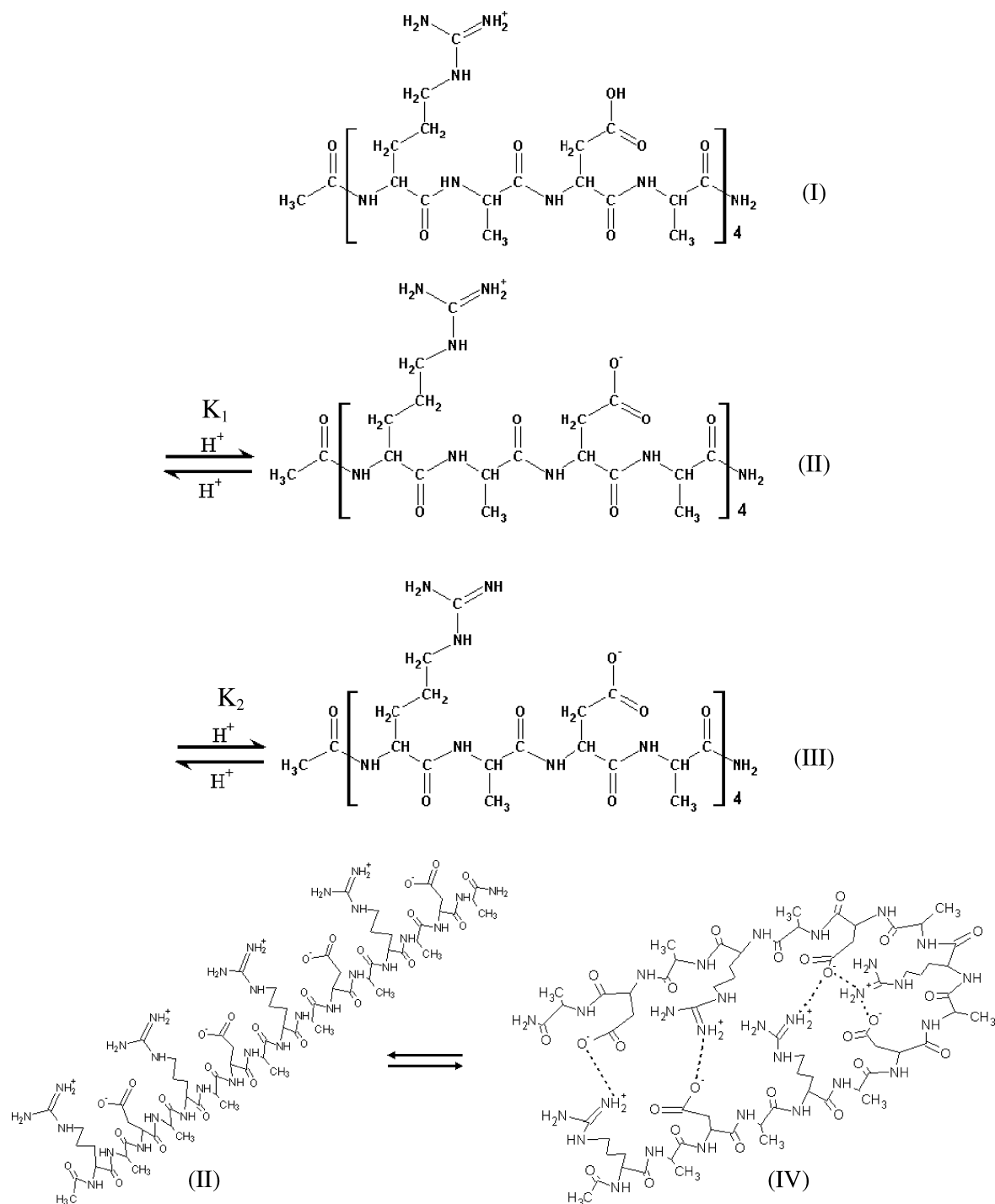
Figure 3 Schematic ionization equations of peptide RADA16-I in aqueous solution. The ion (**I**) is a medium binary acid of peptide, containing the carboxylic methyl substitute and the conjugate acid of the strong basic guanidinium substitute with fully positive charges. The ion (**II**) contained alternating positively and negatively charges at peptide chains and (**III**) was mainly negatively charged, derived from the first ionization and second ionization of (**I**). In the ionic species (**I**), (**II**), and (**III**), the repeated chemical units of protonated or deprotonated peptide RADA16-I were inserted in the black square bracket. The ion-complementary interaction of the intrapeptide (**II**) may be enough to help intrasalt bridge formation (**IV**).

Effect of Heat-Denaturation on Nanofiber Formation

In order to further confirm the above result, we heat-denatured the peptide solutions up to 80 °C and subsequently detected its β-sheet structure changes using circular dichroism (Figure 7). We found that peptide RADA16-I remained in a β-sheet structure (minimum at 215–216 nm and maximum at 195–196 nm) from 25 to 70 °C with 38.6–54.3% high contents (Table 3, S(r) + S(d)), but dramatically decreased 11.3%
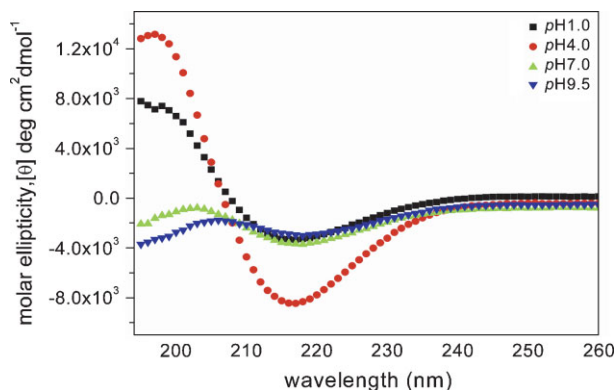
Figure 4 The effect of pH on secondary structures of peptide RADA16-I (100 μM) at various pH values. All the spectra were recorded at 25 °C after incubation overnight at 4 °C and peptide RADA16-I adopted typical β-sheet structure (minimum at 217–218 nm, maximum at 195–206 nm) at pH 1.0–9.5. The color patterns and pH values are shown in the frame.

β-sheet content and increased 14.6% unordered structure content at 80 °C. Interestingly, the RADA 16-I, which lost some of its β-sheet at increasing temperature, was able to regain its β-sheet structure to a significant level immediately back to 25 °C (46.7%) and after three days incubation at 25 °C (data not shown). These data indicate that the thermal denaturation might have only destroyed those ionic and hydrogen bonds responsible for secondary-structure interaction but did not impair covalent interactions of the backbone main chains. Thus, the β-sheet structure and some

good nanofibers can be regained after a slow renaturation process (Figure 8(E) and (F)), although some aggregates still remained (Figure 8(B–E), arrow). The AFM examination showed that heat-denatured peptides were unable to form good nanofiber immediately after heat-denaturation (Figure 8(B–D)), though it contained a good number of β-sheet structures (Figure 7, Table 3), and again confirmed that β-sheet structure was essential, but not sufficient, for nanofiber self-assembly. Higher β-sheet contents or some other physical or chemical complimentary factors are required for nanofiber formation.

Peptide RADA16-I, under moderate pH and heat-denatured conditions, forms a very strong β-sheet structure and self-assembles into long nanofibers and 3D scaffolds. It is known that blood clotting depends on stable and insoluble fibrin fibers, which further mechanically interact with blood cells for hemostasis [22,40,41]. We then tested if the RADA16-I fibers can mimic the naturally occurring process of blood clotting by examining heparin-treated blood (pH = 7.2–7.4) of New Zealand white rabbit ear artery *in vitro* treated with peptide RADA16-I (Figure 9). When 10 mg/ml peptide RADA16-I was added into the blood, the blood cells such as red blood cells (Figure 9(A–C), at black arrow) and white blood cells (Figure 9(A–C), with star) were almost covered by 3D nanofibers matrix of peptide RADA16-I (Figure 9(D)) with only a few emerged, as shown in Figure 9(D) and (E) with black arrow, indicating peptide matrix mechanically netting blood cells. The practically occurring blood hydrogel displayed a jelly morphology and blood flowing out has been
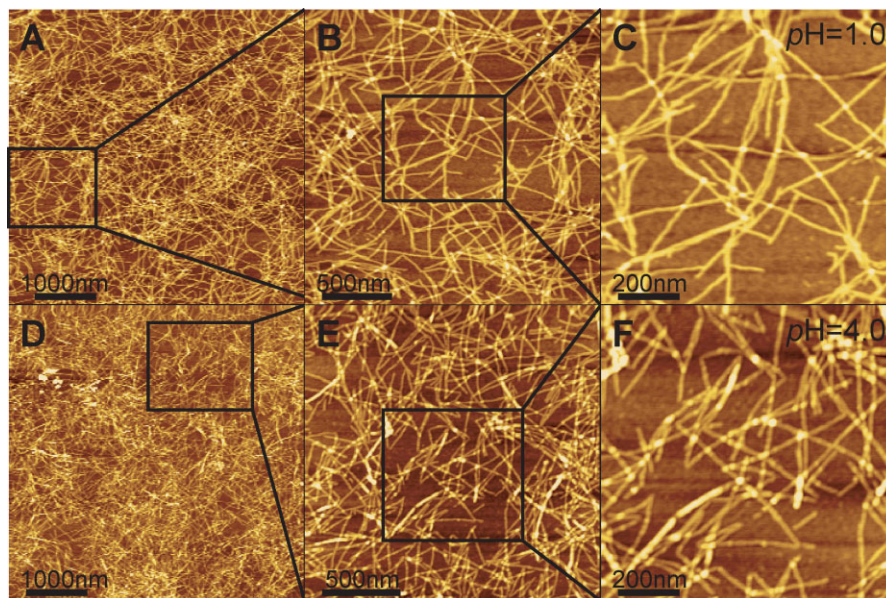

Figure 5 The typical AFM morphological images of 100 μM peptide RADA16-I in pH = 1.0 (A–C) and 4.0 (D–F), large field images (A), (D) and higher magnification of the images inside the black frame (A), (B), (D), and (E). The good 3D nanofiber scaffolds of self-assembling peptide were mediated with decreasing pH values by adding 0.1 M HCl and the typical nanofiber was 17.5 ± 1.13 nm in width, 1.4 ± 0.36 nm in height, and 1108 ± 184 nm in length with 95% confidence. These data are consistent with the previous report.
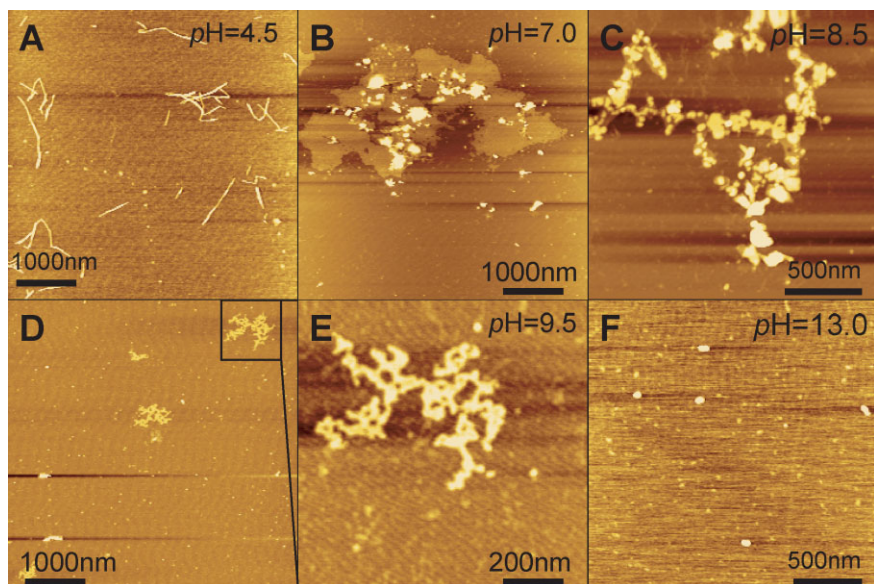
Figure 6   The typical AFM morphological images of 100 μM peptide RADA16-I at different pH values of about 4.5 (A), 7.0 (B), 8.5 (C), 9.5 (D), (E), and 13.0 (F). The morphological changes of self-assembling peptide RADA16-I from nanofiber, filament (A), aggregation (B), (C), (E) to separated globular pieces (D) and (F) were mediated by increasing pH from 4.0 to 13.0 by adding 0.1 M NaOH and 0.1 M HCl.

obstructed because of the formation of network between the peptide-assembled fibers and the cells (white arrow in Figure 9(F)).

DISCUSSION

We examined the pH and temperature-induced secondary-structure transition of the self-assembling peptide RADA 16-I in solution and observed the good
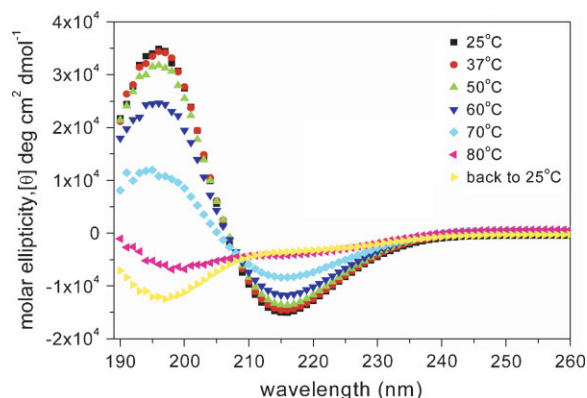

Figure 7   Temperature effect on peptide RADA16-I (100 μM) structural transition in water (pH = 4.0). The peptide RADA16-I adopted a typical β-sheet structure (minimum at 215–216 nm and maximum at 195–196 nm) with decreasing content before 80 °C. The characteristic signal of the β-sheet was still detected, when the temperature was increased from 25 to 80 °C. The random coil (minimum at 197 nm) was observed, when the denatured samples were shifted from 80 to 25 °C. The color patterns and temperature are shown in the frame.

stability of the β-sheet structure at both extreme and moderate ranges of pH and temperature. The peptide lost its β-sheet content at the extreme conditions but held it together in moderate conditions. The morphological properties of peptide RADA 16-I underwent dramatic changes, ranging from the long, extensively interwoven 3D nanofibers, to shorter, less interwoven 3D nanofibers, then to small globular aggregated nanostructures. The hydrogen and ionic bonding among inter- and intrapeptides and water are believed to play a critical role in maintaining the β-sheet structure stability.

Morphological Properties and Ionization of Peptide RADA 16-I in Aqueous Solution

The amphiphilic RADA 16-I peptide is able to exist in three different ionic states: acidic, zwitterionic and basic. In water solution, the peptide had pK_1 1.79, pI 7.20 and pK_2 12.58 and it contained different charges at various pH values (shown in Table 1). Figure 3 shows the molecular species (**I**), which is a medium binary acid of peptide. In pH 1.0 acidic environment, peptide RADA 16-I was mainly positively charged because of arginine residues and aspartic acid residues being protonated. It is possible that the backbone of the peptide chain RADA 16-I would be mutually repulsive and behave like a 'rigid chain', with a little decrease of the characteristic signal of the β-sheet (Figure 4, pH = 1.0, and Table 2). However, the unordered structure and β-turn of peptide RADA16-I, having stable 'rigid chain', should be beneficial for nanofiber formation. On the other hand, nucleation or seeding processes would easily occur and end

Table 3 Estimated structure fractions of heat-denatured peptide RADA16-I

Temperature (°C)	RMSD/NRMSD	Secondary-structure fractions (%)[a]					
		H(r)	H(d)	S(r)	S(d)	Turn	Unrd
25	0.113/0.054	1.3	3.0	39.2	15.1	20.7	20.7
37	0.228/0.045	20.4	1.3	35.1	13.4	14.9	14.9
50	0.185/0.039	18.2	1.1	34.9	13.4	14.8	17.7
60	0.143/0.038	13.8	2.5	33.8	14.3	15.8	19.9
70	0.160/0.080	6.7	4.4	26.3	12.3	21.8	28.5
80	0.151/0.124	0.0	1.6	28.7	14.3	20.1	35.3
	Deviation(+/−)[b]	19.1/1.3	1.4/1.9	0.0/12.9	0.0/2.8	1.1/5.9	14.6/5.8
Back to 25	0.114/0.059	0.1	1.0	31.7	15.0	22.9	29.2

[a] Including six types of secondary structures: H(r) is regular α-helix; H(d) is distorted α-helix; S(r) is regular β-strand; S(d) is distorted β-strand (a partial, but far from complete distortion of the regular β-strand because of the lack of some hydrogen bonds); Turn is β-turn structure; Unrd is unordered structure.
[b] The maximum increase (+) and decrease (−) of secondary-structure fractions (%) compared with those at 25 °C (pure water, pH = 4.0).
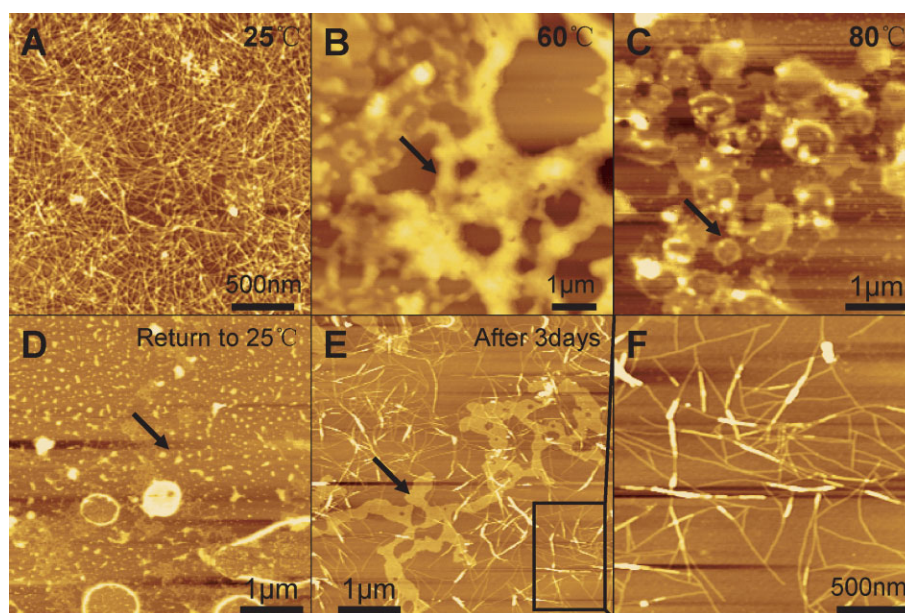

Figure 8 The self-assembling peptide RADA16-I undergoes the morphological changes in response to temperature alternation. The typical AFM height images at 25 °C (A), 60 °C (B), 80 °C (C), back to 25 °C (D), and 3 days later (E), (F). The self-assembling peptide RADA16-I showed the morphological changes from good 3D nanofibers (A), to the aggregated and/or separated globular pieces (B), (C), and (D), to aggregations (E, arrow) and partly 3D nanofibers (E), (F).

up with peptide subunit association to form protofibrils and further elongated filaments or nanofibers.

The molecular species (**II**) contained both positive and negative charges in the peptide chain at pH 4.0. In near neutral pH, the peptide would fully be both positively and negatively charged. It is generally believed that ionic complementarity is mainly responsible for self-assembling peptides because of both electrostatic and hydrophobic interactions. At pH = 7.0, the peptide is very close to its pI. We would expect a long nanofiber formation. However, little nanofiber could be ever detected (Figure 6(B)).

We think that the distorted β-strand [42], β-turn and unordered structure with total 66.4% high contents of zwitterionic peptide, under simple electrolyte such as NaCl salt condition, probably contribute to either intra- or interpeptide salt bridges formation. These attractions among peptides could prevent nanofiber growth in one direction, or bend the peptides (Figure 3, **IV**) for globular aggregation, or initiate the so called 'impurities seeding' process to produce small globular aggregates and fibers, though there exists a considerable amount of regular β-strand (31.5%) structure at pH = 7.0–9.5.
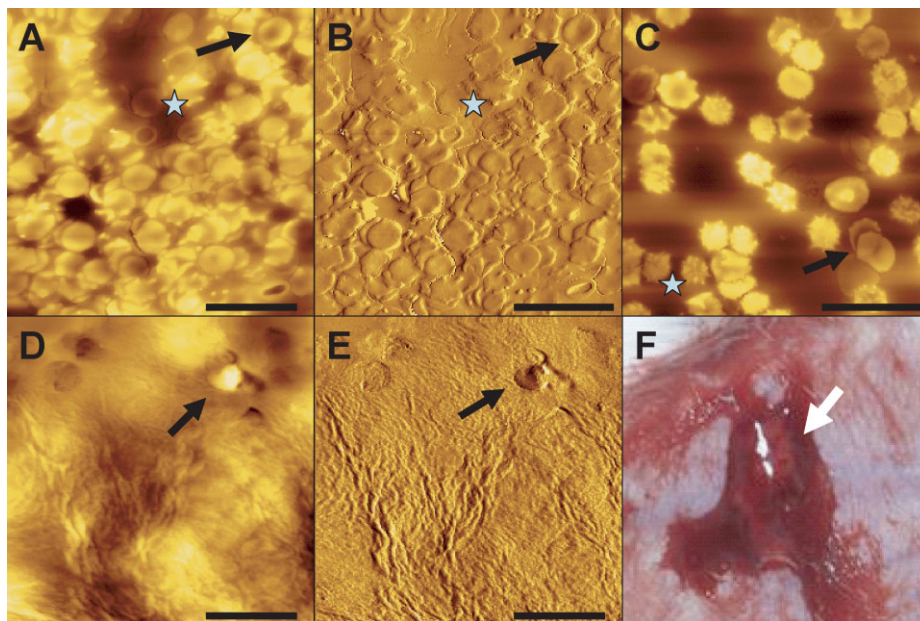
Figure 9   The typical AFM images of hemostatic process and hemostasis of New Zealand white rabbit middle auricular artery. The concaved disc red (black arrow) and lobulated white (star) blood cells, having 6.5–7.5 μm and 7.5–8.5 μm diameter, respectively, are shown in blood (A) and its phase image (B) as well as 10-times diluted blood (C). On adding 10 mg/ml peptide RADA16-I into the blood, these blood cells are almost covered by 3D nanofibers matrix of peptide RADA16-I (D), and only a few (D, E, black arrow) are emerged. Considering the great amount of water in blood, blood-hydrogel formation (like as jelly, white arrow) immediately appears to obstruct blood flowing out (F). Scale bars represent 20 μm.

The molecular species (**III**) was fully negatively charged and was derived from the first ionization and second ionization of (**I**) in pH 9.5 and 13.0 solutions. The peptide would be mainly negatively charged, having high reactive activity (instability), because of strong alkaline arginine and aspartic acid residues being deprotonated. We observed many smaller globular aggregates or short fibers. We believe that at these pH values, the increasing unordered structure prevent the nanofibers formation. On the other hand, the normal charge relationship along the peptide is completely disrupted to lose some complementary charged ions, causing aggregation, as opposed to β-sheet self-assembly, because of the change in active charge distribution along the peptide. In addition, the ion-complementary interaction of the intrapeptide (**II**) may be enough to help intrasalt bridge formation (**IV**). Although intrasalt bridge formation should be relatively difficult because the energy required to bend the backbone of such a short peptide should be relatively large, the existance of β-turn in pH 9.5 and 13.0 solutions should induce intrasalt bridge formation. The outside hydrophobic methyl side chains of the peptide intrasalt (**IV**), as a separated oil bead, held them together to lead to certain macrostructures.

Morphological Properties in Heat-Denatured Conditions

Heat could denature peptide secondary structures of peptide RADA 16-I by destroying noncovalent bonds such as hydrogen or electrostatic interactions. In extreme pH or high-temperature conditions, hydrogen or ionic interactions that have been used to stabilize the β-sheet structures would be impaired. If so, the typical β-sheet structures could be partially impaired with a decrease of 11.3% β-sheet contents as observed by CD measurement and CDPro software analyses (Table 3) from 25 to 80 °C; unordered structure has about 14.6% increase. In addition, heat accelerates the Brownian motion of peptide molecules and decreases chances for peptides to associate with each other by intra- and intermolecular interactions. However, after the temperature was reduced, the peptides would be more hospitable for mutual interaction to self-assemble into nanofibers or any other nanostructure.

Although our data demonstrated that smaller sized ~100–500 nm nanofibers or aggregates occurred in pH 4.5–9.5 solutions, strongly contrasting to those of pH 1.0–4.0, it seems to be inconsistent with the data shown in Figure 9. There are some reasons contributing to the understanding of this hemostasis: first, the blood is a buffer system to be of benefit for nanofiber formation, rather than simple electrolyte such as NaCl salt; second, the higher concentration of peptide RADA16-I such as 10 mg/ml should provide more building blocks for robust nanofibers formation; finally, the buffer ions should be of benefit for gel-network formation.

Our study found that the β-sheet structure was essential, but not sufficient, for nanofiber

self-assembly. Even so, there are still some other physical or chemical factors such as peptide concentration, solvents, different ions as well as buffers to influence self-assembling nanofiber formation. These problems will stimulate us to further investigate them in subsequent study.

Acknowledgements

REFERENCES

1. Zhang S. Fabrication of novel biomaterials through molecular self-assembly. *Nat. Biotechnol.* 2003; **21**: 171–178.

2. Zhang S. Emerging biological materials through molecular self-assembly. *Biotechnol. Adv.* 2002; **20**: 321–339.

3. Zhang S, Marini DM, Hwang W, Santoso S. Design of nanostructured biological materials through self-assembly of peptide and proteins. *Curr. Opin. Chem. Biol.* 2002; **6**: 865–871.

4. Gorman J. On-upping nature's materials: striving for designer substances that build themselves from individual molecules. *Science* 2000; **158**: 364–367.

5. Schachner M. Nervous engineering. *Nature* 2000; **405**: 747–748.

6. Schwartz JJ, Zhang S. Peptide-mediated cellular delivery. *Curr. Opin. Mol. Ther.* 2000; **2**: 162–167.

7. Holmes TC, Lacalle SD, Su X, Liu SS, Rich A, Zhang S. Extensive neurite outgrowth and active synapse formation on self-assembling peptide scaffolds. *Proc. Natl. Acad. Sci. U.S.A.* 2000; **97**: 6728–6733.

8. Zhang S, Altman M. Peptide self-assembly in functional polymer science and engineering. *React. Funct. Polym.* 1999; **41**: 91–102.

9. Zhao X, Zhang S. Self-assembling nanopeptides become a new type of biomaterial. *Adv. Polym. Sci.* 2006; **203**: 145–170.

10. Zhao X, Zhang S. Molecular designer self-assembling peptides. *Chem. Soc. Rev.* 2006; **35**: 1–7.

11. Zhao X, Zhang S. Fabrication of molecular materials using peptide construction motifs. *Trends Biotechnol.* 2004; **22**: 470–476.

12. Zhao X, Nagai Y, Reeves PJ, Kiley P, Khorana HG, Zhang S. Designer short peptide surfactants stabilize G-protein coupled receptor brovine rhodopsin. *Proc. Natl. Acad. Sci. U.S.A.* 2006; **103**: 17707–17712.

13. Zhang S, Holmes TC, Dipersio CM, Hynes RO, Su X, Rich A. Self-complementary oligopeptide matrices support mammalian cell attachment. *Biomaterials* 1995; **16**: 1385–1393.

14. Leon EJ, Verma N, Zhang S, Lauffenburger DA, Kamm RD. Mechanical properties of a self-assembling oligopeptide matrix. *J. Biomater. Sci. Polym. Ed.* 1998; **9**: 297–312.

15. Semino CE, Merok JR, Crane GG, Panagiotakos G, Zhang S. Functional differentiation of hepatocyte-like spheroid structures from putative liver progenitor cells in three-dimensional peptide scaffolds. *Differentiation* 2003; **71**: 262–270.

16. Semino CE, Kasahara J, Hayashi Y, Zhang S. Entrapment of migrating hippocampal neural cells in three-dimensional peptide nanofiber scaffold. *Tissue Eng.* 2004; **10**: 643–655.

17. Bokharia MA, Akaya G, Zhang S, Birch MA. The enhancement of osteoblast growth and differentiation *in vitro* on a peptide hydrogel-polyHIPE polymer hybrid materials. *Biomaterials* 2005; **26**: 5198–5208.

18. Baig CK, Duhamel J, Fung SY, Bezaire J, Chen P. Self-assembling peptide as a potential carrier of hydrophobic compounds. *J. Am. Chem. Soc.* 2004; **126**: 7522–7532.

19. Mira H, Vilar M, Esteve V, Martinell M, Kogan MJ, Giralt E, Salom D, Mingarro I, Penarrubial L, Perez E. Ionic self-complementary induces amyloid-like fibril formation in an isolated domain of a plant copper metallochaperone protein. *BMC Struct. Biol.* 2004; **4**: 7–21.

20. Kisiday J, Jin M, Kurz B, Hung H, Semino C, Zhang S, Grodzisky A. Self-assembling peptide hydrogel fosters chondrocyte extracellular matrix production and cell division: implications for cartilage tissue repair. *Proc. Natl. Acad. Sci. U.S.A.* 2002; **99**: 9996–10001.

21. Scheibel T, Parthasarathy R, Sawick G, Lin XM, Jaeger H. Conducting nanowires built by controlled self-assembly of amyloid fibers and selective metal deposition. *Proc. Natl. Acad. Sci. U.S.A.* 2003; **100**: 4527–4532.

22. Ellis-Behnke RG, Liang YX, Tay DK, Kau PWF, Schneider GE, Zhang S, Wu W, So KF. Nano hemostat solution: immediate hemostasis at the nanoscale. *Nanomedicine: Nanotechnology Biology and Medicine* 2006; **2**(4): 207–215.

23. Zhang S, Holmes T, Lockshin C, Rich A. Spontaneous assembly of a self-complementary oligopeptide to form a stable macroscopic membrane. *Proc. Natl. Acad. Sci. U.S.A.* 1993; **90**: 3334–3338.

24. Lashuel HA, LaBrenz SR, Woo L, Serpell LC, Kelly JW. Protofilaments, filaments, ribbons, and fibrils from peptidomimetic self-assembly: implication for amyloid fibrils formation and materials science. *J. Am. Chem. Soc.* 2000; **122**: 5262–5277.

25. Aggeli A, Nyrkova IA, Bell M, Harding R, Carrick L, Mcleish TCB, *et al.* Hierarchical self-assembly of chiral rod-like molecules as a model for peptide β-sheet tapes, ribbons, fibrils, and fibers. *Proc. Natl. Acad. Sci. U.S.A.* 2001; **98**: 11857–11862.

26. Xiong H, Buckwalter BL, Shieh HM, Hecht MH. Periodicity of polar and nonpolar amino acids is the major determinant of secondary structure in self-assembling oligomeric peptides. *Proc. Natl. Acad. Sci. U.S.A.* 1995; **92**: 6349–6353.

27. Caplan MR, Moore PN, Zhang S, Kamm RD, Lauffenburger DA. Self-assembly of a β-sheet protein governed by relief of electrostatic repulsion relative to van der Waals attraction. *Biomacromolecules* 2000; **1**: 627–631.

28. Yokoi H, Kinoshita T, Zhang S. Dynamic reassembly of peptide RADA16 nanofiber scaffold. *Proc. Natl. Acad. Sci. U.S.A.* 2005; **102**: 8414–8419.

29. Zhang S, Lockshin C, Cook R, Rich A. Unusually stable β-sheet formation in an ionic self-complementary oligopeptide. *Biopolymers* 1994; **34**: 663–672.

30. Zhang S, Rich A. Direct conversion of an oligopeptide from a β-sheet to an α-helix: a model for amyloid formation. *Proc. Natl. Acad. Sci. U.S.A.* 1997; **94**: 23–28.

31. Altman M, Lee P, Rich A, Zhang S. Conformational behavior of ionic self-complementary peptides. *Protein Sci.* 2000; **9**: 1095–1105.

32. Vale'ry C, Artzner F, Robert B, Gulick T, Keller G, Grabielle-Madelmont C, Torres ML, Cherif-Cheikh R, Paternostrey M. Self-assembling process of a peptide in solution: from β-sheet filaments to large embedded nanofibers. *Biophys. J.* 2004; **86**: 2484–2501.

33. Hwang W, Zhang S, Kamm RD, Karplus M. Kinetic control of dimer structure formation in amyloid fibrillogensis. *Proc. Natl. Acad. Sci. U.S.A.* 2004; **101**: 12916–12921.

34. Hartgerink JD, Beniash E, Stupp SI. Peptide-amphiphile nanofibers: a versatile scaffold for the preparation of self-assembling materials. *Proc. Natl. Acad. Sci. U.S.A.* 2002; **99**: 5133–5138.

35. Tjernberg LO, Tjernberg A, Bark N, Shi Y, Ruzsicxka BP, Bus Z, Thyberg J, Callaway DJE. Assembling amyloid fibrils from designed structures containing a significant amyloid β-peptide fragment. *Biochem. J.* 2002; **366**: 343–351.

36. Hong Y, Legge RL, Zhang S, Chen P. Effect of amino acid sequence and *p*H on nanofiber formation of self-assembling peptides EAK16-II and EAK16-IV. *Biomacromolecules* 2003; **4**: 1433–1442.

37. Fung SY, Keyes C, Duhamel J, Chen P. Concentration effect on the aggregation of a self-assembling oligopeptide. *Biophys. J.* 2003; **85**: 537–548.

38. Jun S, Hong Y, Imamura H, Ha BY, Bechhoefer J, Chen P. Self-assembly of the ionic peptide EAK16: the effect of charge distributions on self-assembly. *Biophys. J.* 2004; **87**: 1249–1259.

39. Pang GKH, Baba-Kishi KZ, Patel A. Topographic and phase-contrast imaging in atomic force microscopy. *Ultramicroscopy* 2000; **81**: 35–40.

40. Mankad PS, Codispoti M. The role of fibrin sealants in hemostasis. *Am. J. Surg.* 2001; **182**: 21S–28S.

41. Jackson MR. Fibrin sealants in surgical practice: an overview. *Am. J. Surg.* 2001; **182**(Suppl. 2): 1S–7S.

42. Viseu MI, Carvalho TI, Costa SMB. Conformational transitions in β-Lactoglobulin induced by cationic amphiphiles: Equilibrium studies. *Biophys. J.* 2004; **86**: 2392–2402.